Research Article | Vol. 10, No. 10 / 1 October 2020 / Optical Materials Express 2679
Optical Materials EXPRESS

Reduced optical losses in refractory plasmonic titanium nitride thin films deposited with molecular beam epitaxy

KRISHNA CHAND MAURYA,[1,2,3] VLADIMIR M. SHALAEV,[4] ALEXANDRA BOLTASSEVA,[4] AND BIVAS SAHA[1,2,3,5,6]

[1]*International Centre for Materials Science, Jawaharlal Nehru Centre for Advanced Scientific Research, Jakkur, Bangalore, 560064, India*
[2]*Chemistry and Physics of Materials Unit, Jawaharlal Nehru Centre for Advanced Scientific Research, Jakkur, Bangalore, 560064, India*
[3]*School of Advanced Materials, Jawaharlal Nehru Centre for Advanced Scientific Research, Jakkur, Bangalore, 560064, India*
[4]*School of Electrical and Computer Engineering, and Birck Nanotechnology Center, Purdue University, West Lafayette, IN 47907, USA*
[5]*bsaha@jncasr.ac.in*
[6]*bivas.mat@gmail.com*

Abstract: Refractory plasmonic materials that have optical properties close to those of noble-metals and at the same time are environmentally friendly, commercially viable and CMOS-compatible could lead to novel devices for many thermo-photonic applications. Recently developed TiN thin films overcome some of the limitations of noble-metals, as their optical loss is larger than noble metals and conventional methods to deposit TiN films are not compatible for its integration with other semiconductors. In this work, high-quality epitaxial single-crystalline TiN thin films are deposited with plasma-assisted molecular beam epitaxy (MBE) that exhibit optical losses that are less than that of Au in most part of the visible (300 nm – 580 nm) and near-IR spectral ranges (1000 nm - 2500 nm). In addition, a large figure-of-merit for surface plasmon polariton (SPP) propagation length compared to the previously reported TiN films is achieved with the MBE-deposited films.

1. Introduction

High-temperature-stable plasmonic materials that exhibit metallic behavior with the large real part of the dielectric permittivity (ε_1) and small optical losses (ε_2) are of significant interests for designing efficient emitters and absorbers for solar-thermophotovoltaics (STPV) applications [1–4], transducers in heat-assisted magnetic recording (HAMR) data storage [5,6], structures for hot-carrier photo-catalysis [7,8] as well as photovoltaic devices [9]. In addition to their plasmonic properties and high-temperature stability, such materials should be compatible with standard complementary-metal-oxide-semiconducting (CMOS) technology for photonic interconnects and integrated circuits and should be easily deposited in thin film form with smooth surfaces. Moreover, a variety of energy conversion and optoelectronic device applications also require the integration of plasmonic materials with high-quality semiconductors in heterostructure and superlattice metamaterials with sharp and abrupt interfaces, and in structures that are thermodynamically, morphologically and thermally stable. The well-known noble metals such as Au and Ag though exhibit excellent plasmonic properties [10] in the visible and near-UV spectral ranges, they do not satisfy other important material characteristics as mentioned above. For example, due to the high surface energies, noble metals are difficult to deposit in the ultra-thin film form with sub-nanometer surface roughness. In the case of silver (Ag), the thickness threshold for uniform continuous films is around 12–23 nm [11–13]. Besides, noble metals are not compatible

#405259 https://doi.org/10.1364/OME.405259
Journal © 2020 Received 12 Aug 2020; revised 15 Sep 2020; accepted 15 Sep 2020; published 25 Sep 2020

Optical Materials EXPRESS

with standard CMOS technology and diffuse into Si and other semiconductors, leading to trap states that reduce carrier lifetimes [14–16]. Due to such fabrication and integration challenges, noble metals have thus far found limited real-life applications.

Titanium Nitride (TiN) has emerged as an excellent plasmonic material for visible spectral range applications and exhibit optical properties resembling that of Au in the visible-to-near-IR spectral range [17–36]. Similar to other transition metal nitrides, TiN is hard (hardness of ~ 30 GPa) [37,38], chemically stable, corrosion resistant and exhibit a very high melting temperature of 2930°C that makes it suitable for refractory electronic and plasmonic applications. In addition, due to its ceramic nature, TiN exhibit low index surfaces with surface energies of 24-39 mJ/m^2 [39] that is significantly smaller than the surface energies of noble metals (~ 1-2 J/m^2) [40]. Such lower surface energies allow for uniform TiN thin film depositions with smooth surfaces. Moreover, TiN is CMOS compatible and acts as a buffer layer in the well-established damascene process in integrated circuit (IC) fabrication that makes it suitable as plasmonic and photonic interconnects [41]. Therefore, from the materials fabrication and integration point of view, TiN is an exciting plasmonic material that could lead to novel solutions in many branches of plasmonics and photonics-based modern solid-state device technology.

TiN thin films deposited by sputtering [17–18,20–21,24–28,31,33,36], pulsed laser deposition [35] and atomic layer deposition [22,23,34] exhibit dielectric-to-metallic optical transition characterized by a positive-to-negative change in the real part of the dielectric permittivity (ε_1) in the 450 nm - 500 nm spectral range. Such epsilon-near-zero range can easily be controlled by stoichiometry, deposition conditions and doping [26,42]. Due to its high electron concentrations (~ 5×10^{20} cm^{-3} to ~ 5×10^{21} cm^{-3}), the ε_1 in TiN decreases monotonically with an increase in the wavelength and exhibit low-values between ~ - 80 to - 120 at 2000nm. Such large negative ε_1 are reminiscent of its excellent plasmonic properties, albeit they are smaller than that in Au. The optical loss characterized by the imaginary part of the dielectric permittivity (ε_2) of TiN, however, is larger than in Au primarily due to the interband transitions in the visible spectral range and due to the intraband transitions arising from free carrier (Drude) contributions in the near-IR spectral ranges. The larger optical loss leads to its overall smaller plasmonic figure-of-merits for both propagating surface plasmon polariton (SPP) and localized surface plasmon resonance (LSPR) [43–46] ($FOM_{SPP} = \frac{\varepsilon_1^2}{\varepsilon_2}$ and $FOM_{LSPR} = -\frac{\varepsilon_1}{\varepsilon_2}$) compared to Au. The quality factor $\left(Q = \frac{\omega \frac{\partial \varepsilon_1}{\partial \omega}}{2\varepsilon_2}\right)$ is another important parameter that determines how many optical periods that the free SP oscillation encounter before field decays and also shows how many times the local optical field at the surface of a plasmonic nanoparticle exceeds the external field [47]. Q for sputter-deposited TiN is smaller than that for Au and Ag (see the supplemental document (SD) section-4). In spite of such limitations, several TiN-based plasmonic and photonic structures and devices have been demonstrated recently, such as broadband absorbers and emitters for solar-thermophotovoltaics [2,24], plasmonic interconnects [48], hot-carrier generation [49,50] and non-linear optoelectronics [51] etc. In addition, as experimental Au films are mostly polycrystalline in nature compared to epitaxial TiN, the long-range SPP length in TiN and Au are very similar [52]. Moreover, epitaxial TiN/$Al_{0.72}Sc_{0.28}N$ metal/semiconductor superlattices [53–55] are developed with magnetron sputtering that exhibit both type-I and type-II hyperbolic metamaterial (HMM) [56] dispersion of photonic iso-frequency surfaces and enhanced densities of photonic states.

However, in order to improve TiN performance and device efficiencies further, it is necessary to reduce its optical losses to less than that of the noble metals such as Au. For example, high-losses in sputter-deposited TiN prevent observation of negative refraction in TiN/$Al_{0.72}Sc_{0.28}N$ superlattice HMMs and the optical losses also reduce such HMM's Purcell factor [57] limiting their quantum electronic device efficiencies. Even with the most recent developments in realizing low-loss TiN films [58], large loss in the visible and especially in the near-IR spectral range

Optical Materials EXPRESS

in conventionally grown TiN films remain a challenge. High material losses result in smaller SPP propagation length and hinder TiN's usage for the exploration of its near-zero-index (NZI) properties [42,59] and related optical phenomena, as well as for optimizing TiN devices for applications in solar-thermophotovoltaics and hot-carrier-assisted energy conversion for photo-catalysis, photo-diodes etc. Moreover, as most of the photonic, electronic and optoelectronic applications require integration of TiN with high-quality semiconductors such as GaN in heterostructures with smooth interface and surfaces, suitable and CMOS-compatible deposition methods such as molecular beam epitaxy (MBE) and/or chemical vapor deposition (CVD) needs to be developed for TiN. To date, there are only a handful reports of TiN deposition with MBE method [60,61]. In this article, epitaxial single-crystalline TiN thin films are deposited with ultra-high vacuum (UHV) plasma-assisted MBE and its optical loss is reduced to less than that of Au in the most part of the visible (300 nm – 580 nm) and near-IR spectral ranges (1000 nm - 2000nm). Temperature-dependent plasmonic properties are characterized in the temperature range from 100 K to 700 K, and the results are explained with traditional Drude model of the dielectric permittivity. Finally, the optical and material properties of MBE-deposited TiN thin films are compared with sputter-deposited TiN and with noble metals such as Au. Demonstration of high-quality epitaxial TiN films utilizing MBE as well as the reduction of TiN optical loss to less than that of conventional gold films in most of the visible and near-IR spectral range could pave the way for TiN's integration with main-stream semiconductors for novel, efficient photonic and optoelectronic devices.

2. Growth and characterization methods

TiN thin films were deposited with UHV-PAMBE on (001) MgO and (0001) Al_2O_3 substrates at a base-pressure of 1×10^{-10} Torr and growth temperature of 600°C. The MBE system was enabled with a load-lock and a sample preparation chamber that operated at a base-pressure of 1×10^{-9} Torr for substrates cleaning. Prior to the deposition and after the cleaning of the substrates with wet-chemicals (acetone and methanol), the substrates were thermally cleaned inside the prep-chamber at 600°C for 1 hour. Substrates were then transferred to the growth chamber and were further thermally cleaned at 800°C for 2 hours before the growth temperature was lowered to 600°C. Ti metal (with a purity of 99.999%) was evaporated from a TiC-coated graphite effusion cell at 1500°C that resulted in a beam-equivalent pressure of 5×10^{-8} Torr and plasma-activated nitrogen source (purity of 99.99999%) was used with 375 W rf-power and 1.5 sccm of nitrogen gas flow. Multiple films with different layer thicknesses (20 nm, 80 nm and 120 nm) were deposited with the growth rate of 0.5 nm/min. The dielectric permittivity does not change significantly in this thickness range (see SD Fig.S6). However, the main results in this work are presented from a film with 80 nm of thickness.

High-resolution X-ray diffraction (HRXRD) studies were performed with Bruker D8 thin film XRD machine, while the field-emission scanning electron microscopy (FESEM) and atomic force microscopy (AFM) imagining were performed with FEI Inspect F50 and Bruker Innova respectively. All optical characterizations were performed with J. A. Woollam RC2 ellipsometer attached with a cryostat operating from 100K-800 K temperature range. Details about the characterization method are presented in the SD section.

3. Structural characterization

HRXRD spectra (see Fig. 1(a) and (b)) show that MBE deposited TiN thin films grow with 002 orientations on the (001) MgO substrates (TiN/MgO) and with 111 orientations on the (0001) Al_2O_3 substrates (TiN/Al_2O_3) respectively. The TiN/MgO film exhibit a small mosaicity characterized by a full-width-at-the-half-maxima (FWHM) of the rocking curve of 0.19°. The rocking curve FWHM of TiN/Al_2O_3 was found to be even smaller at 0.03° that indicated its superior crystalline properties. An out-of-plane (c-axis) lattice parameter of 4.25Å was

Optical Materials EXPRESS

determined for the TiN/MgO, while the same for TiN/Al_2O_3 was 4.24Å . Since TiN is essentially lattice-matched with MgO (lattice constant of 4.21Å), TiN/MgO grows as a nominally single-crystalline film with [001] (001) TiN || [001] (001) MgO epitaxial relationship. Epitaxy is also characterized by asymmetric φ-scan measurements that show four equally spaced φ-peaks for TiN (111) on MgO substrates demonstrating four-fold in-plane rotational symmetry (see SD-7). The epitaxial relationship of TiN/Al_2O_3, on the other hand, was found to be (111) TiN || (0001) Al_2O_3. Similar epitaxial relations have been seen in plasma-enhanced atomic layer deposited TiN film on MgO and Al_2O_3 substrates [62].

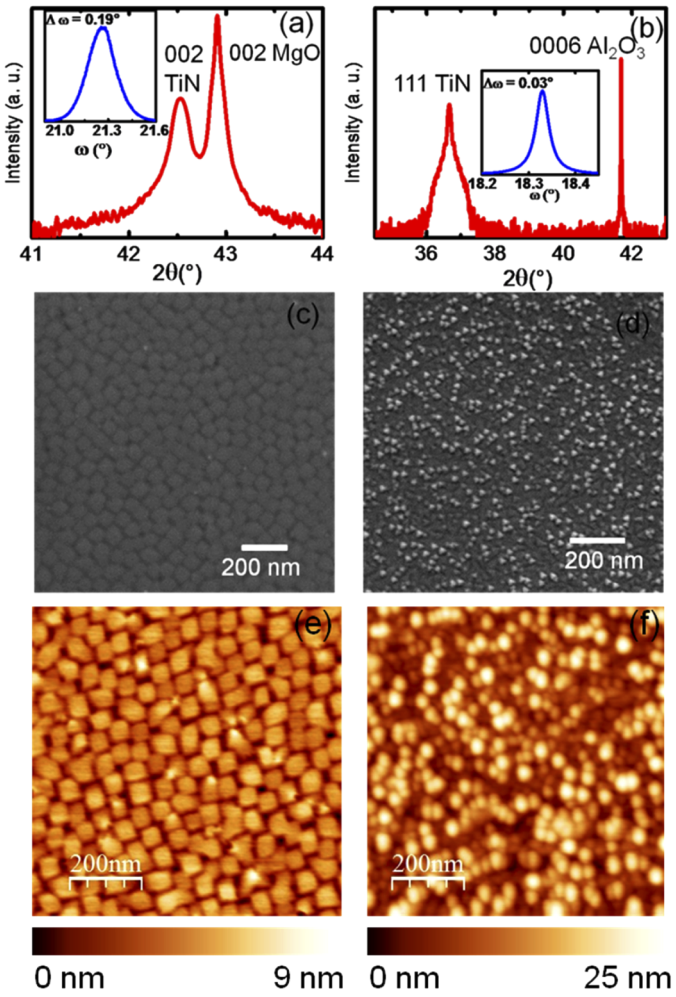

Fig. 1. Symmetric $2\theta - \omega$ X-ray diffraction spectrum of TiN/MgO (a) and TiN/Al_2O_3 (b) thin films along with their rocking curve (ω-scan) in the inset. TiN on MgO substrate was found to grow with 002 orientations, while on Al_2O_3 substrates, TiN grow with 111 orientations. Plan-view FESEM images of the TiN/MgO (c) surface exhibit mount features with four-fold symmetry, while the TiN/Al_2O_3 (d) film exhibit pyramidal structures with 111 oriented growth. Atomic force micrographs of the films are presented that exhibit rms. surface roughness of (e) 1.2 nm in TiN/MgO film and (f) 3.8 nm in TiN/Al_2O_3 film respectively.

Plan-view FESEM image of TiN/MgO film exhibit (see Fig. 1(c)) square-shaped densely packed features with an average feature size of ~ 60 nm. Such square-shaped structure arises

Optical Materials EXPRESS

from the formation of kinetically driven mound structures that were also observed previously in semiconductors such as ScN and TiN deposited with magnetron sputtering [63–64]. Formations of such mounds are related to an Ehrlich-Schwoebel surface diffusion barrier that inhibits adatom migration down steps promoting nucleation on the terraces. As the growth continues, such mounds connect along the edges with the development of the cusps. Reduced adatom mobility at cusps and shadowing during the further deposition led to the nano-pipe formation along the mound edges and surface roughening [63]. The mounds structures exhibit four-fold symmetry as expected for the nucleation of rocksalt crystal structure representing the growth front of TiN. The surface RMS-roughness of TiN/MgO exhibited a small value of 1.2 nm (Fig. 1(e)).

Plan-view FESEM image of the TiN/Al_2O_3 film, on the other hand, showed pyramidal features with an average pyramid size of ~ 20 nm, which is consistent with its 111 oriented growth and crystal symmetry. Such pyramidal grain growths were observed previously for sputter-deposited TiN films deposited on sapphire substrates. The RMS-surface roughness of the TiN/Al_2O_3 film (see Fig. 1(f)) was slightly larger at 3.8 nm, compared to the films deposited on MgO substrates.

4. Optical characterization

4.1. Ambient temperature optical characterization

The ambient temperature optical characterization of the films was performed with spectroscopic ellipsometer in the reflection mode at three different angles (55°, 65° and 75°) of incidences and the experimental (ψ, Δ) spectra were fitted with a combination of Drude-Lorentz model [65] (see Eq. (1)) comprising three Lorentz oscillators that fitted the data well.

$$\varepsilon(\omega) = \varepsilon_1 + i\varepsilon_2 = \varepsilon_\infty - \frac{\omega_p^2}{\omega^2 + i\Gamma_D\omega} + \sum_{j=1}^{3} \frac{\omega_{L,j}^2}{\omega_{0,j}^2 - \omega^2 - i\gamma_j\omega} \quad (1)$$

Where, $\varepsilon_\infty$is the high-frequency dielectric constant, ω_p and Γ_D are the plasma frequency and Drude damping constant respectively. $\omega_{L,j}^2 = f_j\omega_{0,j}\gamma_j$; f_j, $\omega_{0,j}$ and γ_j describe the Lorentz oscillator strength, resonant energy, and damping factor, respectively. The real part of permittivity (ε_1) signifies the optical response and the imaginary part of permittivity (ε_2) is the optical loss of the material. The measurement spectral range from 210 nm to 2500 nm corresponds to most of the solar spectrum and was also limited by the instrument. Details about the measurement technique and data fitting analysis are presented in the SD.

Ellipsometry data-fitting showed that TiN film deposited on both substrates exhibit a transition from positive-to-negative ε_1(see Fig. 2(a)) representative of the onset of their metallic nature near 470 nm that is consistent with previous reports of the sputter-deposited TiN thin film. With an increase in wavelength, ε_1 decreased monotonically and exhibited a minimum of –165 and –127 respectively at 2500 nm for the TiN/MgO and TiN/Al_2O_3 films respectively. Films deposited on MgO substrate exhibited higher negative ε_1 compared to the films deposited on Al_2O_3 substrate at long-wavelengths mostly due to their higher carrier concentrations (see SD). As large ε_1 are necessary [17] for achieving higher optical figure-of-merits and consequently leads to higher efficiencies in solar-energy conversion devices (that mostly operate in the 200 nm to 2500 nm spectral range), TiN would be ideally suited for such purpose. Optical loss or ε_2 of the films were also found to increase with an increase in the wavelength (see Fig. 2(b)), with TiN/Al_2O_3 exhibiting significantly smaller losses compared to the TiN/MgO. The lower ε_2 in TiN/Al_2O_3 compared to TiN/MgO is due to the smaller Drude damping constants in TiN films deposited on Al_2O_3 substrates compared to the ones deposited on MgO substrates (see Fig. 4 for detailed discussion). Smaller Drude damping constant in TiN/Al_2O_3 arises from its better crystalline quality as evidenced by the lower FWHM of the rocking curve in HRXRD. In addition, the ω_p in TiN/Al_2O_3 is also smaller than TiN/MgO that provides smaller ε_2. At 470 *nm* (i.e. at the cross-over wavelength), ε_2 in TiN/Al_2O_3 exhibit a value of 2.0, while the same for TiN/MgO is

Optical Materials EXPRESS

2.5 that amounts to a 25% smaller value. The lower optical loss ε_2 in TiN would help to achieve better near-zero-index (NZI) properties [71] that are necessary for the demonstration of exotic optical phenomena such as light tunneling [66], diverging velocity [67], optical time reversal [68], frequency shifting [67], time refraction [69,70]. It also helps to improve the hot-carrier energy transport and conversion efficiencies for photo-catalysis, photo-thermal energy conversion, solar-thermophotovoltaics etc. [2,7,9,72]. In addition, lower optical losses in TiN/Al_2O_3 in the near-IR spectral range will help develop improved TiN-based SPP and plasmonic interconnects [7,13,58] with functionalities at the telecommunication wavelength (~ 1500 nm).

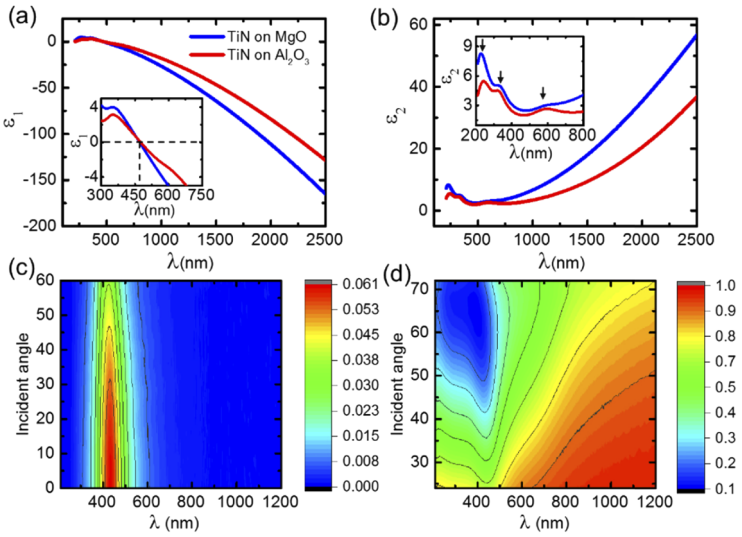

Fig. 2. (a) The real (ε_1) and (b) imaginary (ε_2) part of the dielectric permittivity of MBE-deposited TiN thin film on MgO and Al_2O_3 substrates are presented. The inset show that TiN becomes plasmonic at 470 nm spectral range, while the optical loss in the visible spectral range to be much smaller on films deposited on Al_2O_3 substrates compared to the MgO substrate. There are three peaks in 200-800 nm range which arises from interband transitions (shown in inset). (c) Transmission and (d) reflection spectrum (is plotted as a ratio between the *p*-polarized and the *s*-polarized light.) of TiN/Al_2O_3 are presented as a function of wavelength and the angle of incidence. Transmission exhibits a peak and reflection shows a sharp dip near the crossover wavelength (or near the plasma frequency). Brewster angle (near 65°) at reflection spectrum can be clearly visible.

To validate ellipsometry data-fitting and to better understand plasmonic properties, reflection (R) and transmission (T) measurements were performed as a function of the angle of incidence. Since the results are qualitatively very similar, R and T spectrum from TiN/Al_2O_3 film is presented in Fig. 2(c) and 2(d), while the result from the TiN/MgO could be found in SD (Fig. S4). Representative of the onset of TiN's metallic character, transmission measurement (see Fig. 2(c)) showed a clear and distinct peak at ~ 430 nm that corresponds to its transition from positive ε_1(dielectric nature) to negative ε_1 (metallic nature). Transmittance decreased with an increase in the angle of incidence as expected and vanished away from the peak position, where reflectivity becomes maximum. Reflectivity presented as a ratio between the *p*-polarized and *s*-polarized light showed near unity values in most of the visible to near-IR spectral range except for transition regions when the reflectance exhibited a sharp dip near the crossover wavelength. The Brewster angle is clearly visible ~65° in the reflection spectrum.

Optical Materials EXPRESS

4.2. Temperature-dependent optical characterization

Having analyzed the plasmonic properties at ambient temperature (300 K), the temperature-dependent optical properties were measured with a cryostat from 100K-700 K temperature range at 70° angle of incidence. The cryostat chamber was attached with a turbo-molecular pump leading to a chamber pressure of 10^{-7} to 10^{-6} Torr that would reduce possibilities of oxidation. The measured experimental (ψ, Δ) spectrum as a function of temperature was fitted with Eq. (1) and results are presented in Fig. 3.

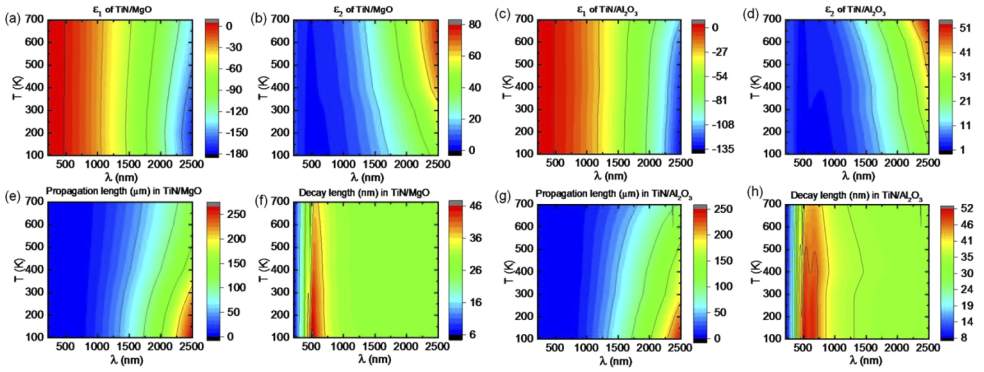

Fig. 3. Temperature-dependent plasmonic properties, (a) and (c) real component of the dielectric constant (ε_1), (b) and (d) imaginary component of the dielectric constant (ε_2), (e) and (g) SPP propagation length and (f) and (h) plasmon decay length (or penetration length) of the MBE-deposited TiN/MgO and TiN/Al_2O_3 thin films are presented respectively as a function of the wavelength. With an increase in temperature (100K-700 K), ε_1 was found to decrease, while ε_2 increases due to an increase in Drude damping constants and plasma frequency.

Temperature-dependent measurements showed that the real component of the dielectric permittivity (ε_1) decreased slightly (see Fig. 3(a) and Fig. 3(c)) with an increase in temperature, while the optical loss or ε_2 increased significantly (see Fig. 3(b) and Fig. 3(d)) over the same temperature range. The changes in the optical constants were observed primarily in the near-IR spectral regions, where the interband transitions are expected to be less important and the free-carrier Drude contribution is significant (see the SD). The temperature-dependence of the dielectric constant can be well-explained by the Drude theory, which contains plasma frequency (ω_p) and damping constant (Γ_D). The ω_p is related to the carrier concentration (N) and effective mass (m^*) through the equation $\omega_p^2 = \frac{Ne^2}{m^*\epsilon_0}$. With an increase in temperature, the carrier density (N) usually decreases due to the volume expansion following a relation $N = \frac{N_0}{1+\gamma(T-T_0)}$ where, γ is the volume thermal expansion coefficient, the electron effective mass decreases [73]. On the other hand, Γ_D depends on various carrier scattering mechanisms such as electron-electron scattering, electron-phonon scattering, etc. [74–78]. As the temperature increases, the scattering rates also increase, and consequently Γ_D increases.

The Γ_D and ω_p have been extracted from the temperature-dependent experimental data-fitting and presented in Fig. 4 that highlights its increasing trend with an increase in temperature. The small decrease in ε_1 at long-wavelength regions with the increase in temperature is related to both ω_p as well as the Γ_D through the relationship $\varepsilon_1 = \frac{-\omega_p^2}{\omega^2+\Gamma_D^2}$. Since the value of ω_p is lesser in TiN/Al_2O_3 film compare to TiN/MgO, that's why ε_1 is higher in TiN/Al_2O_3 film in comparison to TiN/MgO. The optical loss (ε_2) is also related to the Γ_D and ω_p through the relationship $\varepsilon_2 = \frac{\omega_p^2\Gamma_D}{\omega^3+\Gamma_D^2\omega}$. The increment in Γ_D and ω_p with temperature is responsible for

Optical Materials EXPRESS

the increment in ε_2. Results show that Γ_D and ω_p is smaller in MBE-deposited TiN/Al_2O_3 film compared to the TiN/MgO (see Fig. 4), consequently, ε_2 is lesser in TiN/Al_2O_3 than TiN/MgO. As discussed before, the lower Γ_D in TiN/Al_2O_3 film is due to its better crystalline quality, while the smaller ω_p is associated with its lower carrier concentrations. Similar observation about the temperature-dependence of ε_1 and ε_2 for sputter-deposited TiN thin films [79,80], Au [81] and Ag [82] are also made recently. It should be mentioned that though the ε_2 of the MBE-deposited TiN films increases with the increasing temperature, the extent of such increase is much smaller than that observed in sputter-deposited TiN films on Al_2O_3 [79] and MgO [80] substrates. For example, previous reports have shown that with an increase in temperature from room temperature to 900°C, the ε_2 almost doubled for a sputter-deposited TiN/MgO at 2000nm [79], while in the MBE-deposited film, with an increase in temperature from 100 K to 700 K, at 2000nm the ε_2 increased by ~ 33%. Since high-temperature applications require plasmonic materials with low optical losses at elevated temperatures, the MBE-deposited TiN, therefore, should be better suited for real-life applications.

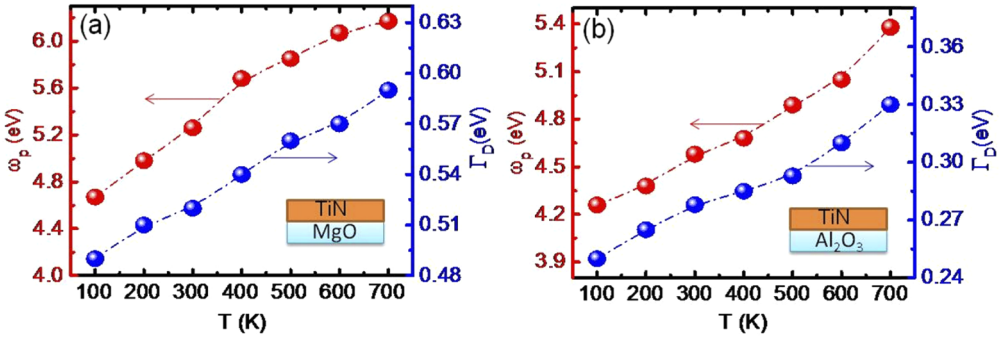

Fig. 4. Temperature-dependent plasma frequency (ω_p) and Drude damping factor (Γ_D) of (a) TiN/MgO, (b) TiN/Al_2O_3 films. The Γ_D and ω_p increases monotonically with the increase in temperature from 100K-700K, which explains the increase of losses (ε_2) with temperature and decrease in ε_1. The values of Γ_D and ω_p are lesser in TiN/Al_2O_3 film compare to TiN/MgO, resulting in lesser losses (ε_2) in TiN/Al_2O_3 film compared to TiN/MgO film. The lines drawn through the data are meant to guide the eye.

In addition to the optical constants, the SPP propagation length (L) at TiN-air interfaces and plasmon-decay length (δ) in the metal (or penetration depth) were also calculated from the experimental dielectric permittivity. The SPP propagation constant in the direction of propagation can be written as [83,84]

$$k_x = \frac{2\pi}{\lambda}\sqrt{\frac{\varepsilon_M \varepsilon_D}{\varepsilon_M + \varepsilon_D}} \tag{2}$$

Where $\varepsilon_M = \varepsilon_1 + i\ \varepsilon_2$ is the dielectric function of TiN, ε_D is the dielectric function of dielectric medium (air in this case).The propagation length (L) is defined as the distance for the SPP intensity to decay by a factor of *1/e*.

$$L = \frac{1}{2\ Im(k_x)} \tag{3}$$

As expected TiN turns plasmonic after ~ 470 nm, the SPP propagation starts and increases monotonically with the increase in the wavelength and exhibit a large value of ~ 268μm in TiN/MgO film and ~ 246μm in TiN/Al_2O_3 film at 100K temperature at 2500 nm (see Fig. 3(e) & Fig. 3(g)). With an increase in the temperature, as the ε_1 decreases with associated ε_2 increase, the SPP propagation length also decreases, but nevertheless, always exhibit large numbers of more than 110 μm at 2500 nm at 700 K. In previously reported TiN thin films deposited by

Optical Materials EXPRESS

atomic layer deposition and sputtering on Si [85] and Al_2O_3 [86] substrates, the observed SPP propagation length was less than 20 μm at room temperature at the wavelength of 1500 nm, while the MBE-deposited TiN thin films in this study exhibit the SPP propagation length of ~58 μm on the TiN/MgO film and ~56 μm on the TiN/Al_2O_3 film at room temperature at the same telecommunication wavelength of 1500nm. Therefore, these are the highest SPP propagation length reported in TiN films to the best of our knowledge.

The plasmon decay length (δ) (when electric field falls off evanescently perpendicular to the TiN surface) is calculated as [84]

$$\delta = \frac{2\pi}{\lambda}\sqrt{\frac{|\varepsilon_1| + \varepsilon_D}{|\varepsilon_M|^2}} \tag{4}$$

Results show that the decay length is maximum near the crossover wavelength as expected and decreases (10-15%) with an increase in temperature (see Fig. 3 (d)). The large plasmon decay length of 40-50 nm in the visible spectral range is a manifestation of TiN's very good plasmonic property. Since the decay length is a key parameter for deciding the thickness of many photonic devices, for example, the thickness of superlens [87], such a larger value of decay length will make possible TiN-based photonic structures.

4.3. Comparison of MBE-deposited TiN with noble metals

Having discussed the structure and optical properties of MBE-deposited single-crystalline TiN thin film on MgO and Al_2O_3 substrates, a comparison of its optical properties with noble metals

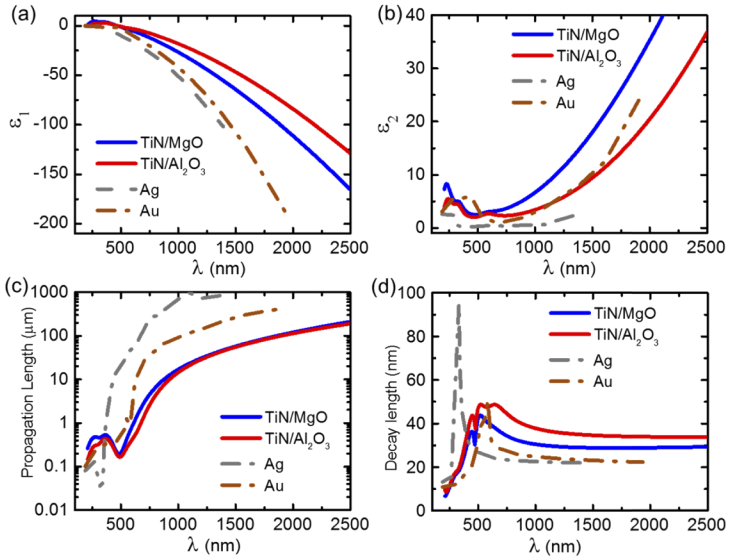

Fig. 5. The real (ε_1, (a)) and imaginary (ε_2, (b)) parts of the dielectric permittivity of MBE-deposited TiN thin film on Al_2O_3 and MgO substrate at room-temperature are presented. Plotted in the same figure are the optical constants of noble metals such as Au and Ag that are adopted from Johnson and Christy et al. [88]. The figure shows that though the ε_1 of TiN is larger, they are still smaller than Au. While the optical loss (ε_2) of TiN/Al_2O_3 is smaller than that of the Au in most of the visible to near-IR spectral range. (c) SPP propagation length (L) and (d) plasmon decay length (δ) inside TiN is calculated along with the same for Au and Ag. As shown in the figure, the SPP propagation length in TiN/Al_2O_3 is almost as large Au in high-wavelength regions, while the plasmon decay lengths are higher in TiN.

Optical Materials EXPRESS

(such as Au and Ag) are presented in this section. As discussed before, noble metals such as Au possess several material challenges that limit their device applications, especially at high temperatures. While TiN successfully overcomes most of these material challenges, in terms of the optical properties, the ε_1 of TiN is smaller than that of the Au (and Ag). The difference in the magnitude of ε_1 is much smaller in the visible spectral range (see Fig. 5(a)), but increases monotonically and rapidly with the increase in wavelength in the near-IR range mostly due to its lower carrier concentrations than Au. The optical losses (ε_2) of MBE-deposited TiN/Al_2O_3 developed here, however, are less than that of Au in most of the visible (300-580 nm) and near-IR spectral range (1000-2000nm) (see Fig. 5(b)), which is an important finding in this work. Contrary to the TiN/Al_2O_3, the optical loss in TiN/MgO is though smaller than Au in the visible (300-580 nm) spectral range but is significantly larger in the near IR range that is consistent with previous sputter-deposited TiN on MgO substrates [17]. The smaller optical loss in TiN/Al_2O_3 translates into larger SPP propagation lengths (see Fig. 5(c)). The plasmon decay length inside TiN (see Fig. 5(d)) is larger in TiN/Al_2O_3 compared to both the TiN/MgO and Au that makes it a suitable candidate for several photonic applications. However, comparison of the plasmonic figure-of-merits, namely $FOM_{SPP,}$ FOM_{LSPR}, and Q between the noble metals (Au and Ag) and MBE-deposited TiN show that further improvement of TiN's properties would be required for some applications. Optical properties of the MBE-deposited TiN thin film were compared with the previous reports on low-loss TiN manufactured by both dc magnetron sputtering [18] and MBE [61] methods (see SD section-8). Figure S8 shows that the optical loss (ε_2) is almost the same in the 210 nm – 600 nm wavelength region, however, the present MBE-deposited TiN/Al_2O_3 film exhibit almost 2 times lower ε_2 in the 600 nm – 2500 nm wavelength region that is the lowest optical loss reported in TiN films to date in this spectral range.

5. Conclusion

In conclusion, epitaxial single-crystalline TiN thin films are deposited with ultra-high vacuum plasma-assisted molecular beam epitaxy (UHV-PEMBE) that exhibit reduced optical losses compared to the previously reported MBE and sputter-deposited TiN thin films. Comparative analysis of plasmonic figures-of-merit reveals that the MBE-deposited TiN films support surface plasmon-polaritons with the longer propagation lengths at TiN-air interfaces than those in the sputter-deposited TiN thin film. Materials characterization showed that the TiN films grow as nominally single-crystalline materials with very small full-width-at-the half-maxima of the rocking curve and smooth surfaces. Consistent with our previous studies, the temperature-dependent plasmonic properties exhibit a monotonic decrease in the real part of the dielectric permittivity (ε_1) and an increase in the optical losses (ε_2) that can be attributed to the increased Drude damping constants with the increase in the temperature. The lower optical loss in TiN/Al_2O_3 compared to Au in most of the visible-to-near-IR spectral range would enable low-loss SPP propagation in improved plasmonic devices. The development of MBE-deposited TiN thin films with reduced optical losses could enable its integration with III-V semiconductors such as GaN, InN etc. and lead to TiN-based photonic/plasmonic on-chip devices, broad-band light absorbers and emitters for solar-thermophotovoltaics and hot-carrier-assisted devices with improved efficiencies.

Acknowledgement

KCM and BS thank International Centre for Materials Science and Sheikh Saqr Laboratory for support. BS thanks the Science and Engineering research board (SERB) Start-up grant SRG/2019/000613 from the Department of Science and Technology, India for partial financial assistance. KCM thanks to Mr. Abhijit Chatterjee, Mr. Bidesh Biswas, Mrs. Dheemahi Rao and Mr. Mahesh for assistance with MBE growth, XRD, SEM and AFM respectively.

Optical Materials EXPRESS

Disclosures

The authors declare that there are no conflicts of interest related to this article.

See Supplement 1 for supporting content.

References

1. W. Spirkl and H. Ries, "Solar thermophotovoltaics: An assessment," J. Appl. Phys. **57**(9), 4409–4414 (1985).
2. H. Wang, Q. Chen, L. Wen, S. Song, X. Hu, and G. Xu, "Titanium-nitride-based integrated plasmonic absorber / emitter for solar thermophotovoltaic application," Photonics Res. **3**(6), 329–334 (2015).
3. C. Chang, W. J. M. Kort-kamp, J. Nogan, T. S. Luk, A. K. Azad, A. J. Taylor, D. A. R. Dalvit, M. Sykora, and H. Chen, "High-Temperature Refractory Metasurfaces for Solar Thermophotovoltaic Energy Harvesting," Nano Lett. **18**(12), 7665–7673 (2018).
4. Y. Wang, H. Liu, and J. Zhu, "Solar thermophotovoltaics: Progress, challenges, and opportunities Solar thermophotovoltaics: Progress, challenges, and opportunities," APL Mater. **7**(8), 080906 (2019).
5. W. A. Challener, C. Peng, A. V. Itagi, D. Karns, W. Peng, Y. Peng, X. Yang, X. Zhu, N. J. Gokemeijer, Y. Hsia, G. Ju, R. E. Rottmayer, M. A. Seigler, and E. C. Gage, "Heat-assisted magnetic recording by a near-field transducer with efficient optical energy transfer," Nat. Photonics **3**(4), 220 (2009).
6. N. Zhou, X. Xu, A. T. Hammack, B. C. Stipe, K. Gao, W. Scholz, and E. C. Gage, "Plasmonic near-field transducer for heat-assisted magnetic recording," Nat. Photonics **3**(3), 141–155 (2014).10.1515/nanoph-2014-0001
7. P. Christopher, "Singular characteristics and unique chemical bond activation mechanisms of photocatalytic reactions on plasmonic nanostructures," Nat. Mater. **11**(12), 1044–1050 (2012).
8. W. Ahn, I. Vurgaftman, J. J. Pietron, and B. S. Simpkins, "Energy-tunable photocatalysis by hot carriers generated by surface plasmon polaritons," J. Mater. Chem. A **7**(12), 7015–7024 (2019).
9. H. A. Atwater and A. Polman, "Plasmonics for improved photovoltaic devices," Nat. Mater. **9**(3), 205–213 (2010).
10. H. A. Atwater, "The Promise of Plasmonics," Sci. Am. **296**(4), 56–62 (2007).
11. W. Chen, M. D. Thoreson, S. Ishii, A. V. Kildishev, and V. M. Shalaev, "Ultra-thin ultra-smooth and low-loss silver films on a germanium wetting layer," Opt. Express **18**(5), 5124 (2010).
12. V. J. Logeeswaran, N. P. Kobayashi, M. S. Islam, W. Wu, P. Chaturvedi, N. X. Fang, S. Y. Wang, and R. S. Williams, "Ultrasmooth silver thin films deposited with a germanium nucleation layer," Nano Lett. **9**(1), 178–182 (2009).
13. P. R. West, S. Ishii, G. V Naik, N. K. Emani, and V. M. Shalaev, "Searching for better plasmonic materials,," Laser Photonics Rev. **4**(6), 795–808 (2010).
14. G. Bemski, "Recombination properties of gold in silicon," Phys. Rev. **111**(6), 1515–1518 (1958).
15. C. B. Collins and R. O. Carlson, "Properties of Silicon Doped with Iron or Copper," Phys. Rev. **108**(6), 1409–1414 (1957).
16. L. D. Yau and C. T. Sah, "Measurement of trapped-minority-carrier thermal emission rates from Au, Ag, and Co traps in silicon," Appl. Phys. Lett. **21**(4), 157–158 (1972).
17. G. V Naik, V. M. Shalaev, and A. Boltasseva, "Alternative Plasmonic Materials: Beyond Gold and Silver," Adv. Mater. **25**(24), 3264–3294 (2013).
18. G. V. Naik, B. Saha, J. Liu, S. M. Saber, E. A. Stach, J. M. K. Irudayaraj, T. D. Sands, V. M. Shalaev, and A. Boltasseva, "Epitaxial superlattices with titanium nitride as a plasmonic component for optical hyperbolic metamaterials," Proc. Natl. Acad. Sci. U. S. A. **111**(21), 7546–7551 (2014).
19. E. Pascual and J. Esteve, "Surface reflectivity of TiN thin films measured by spectral ellipsometry," Surf. Sci. **251-252**, 200–203 (1991).
20. P. Patsalas and S. Logothetidis, "Optical, electronic, and transport properties of nanocrystalline titanium nitride thin films," J. Appl. Phys. **90**(9), 4725–4734 (2001).
21. K. Postava, M. Aoyama, and T. Yamaguchi, "Optical characterization of TiN/SiO2 (1000 nm)/Si system by spectroscopic ellipsometry and reflectometry," Appl. Surf. Sci. **175-176**, 270–275 (2001).
22. H. Van Bui, A. Y. Kovalgin, and R. A. M. Wolters, "On the difference between optically and electrically determined resistivity of ultra-thin titanium nitride film," Appl. Surf. Sci. **269**, 45–49 (2013).
23. J. A. Briggs, G. V. Naik, T. A. Petach, B. K. Baum, D. Goldhaber-gordon, A. Jennifer, J. A. Briggs, G. V. Naik, T. A. Petach, B. K. Baum, D. Goldhaber-gordon, and J. A. Dionne, "Fully CMOS-compatible titanium nitride nanoantennas," Appl. Phys. Lett. **108**(5), 051110 (2016).
24. W. Li, U. Guler, N. Kinsey, G. V. Naik, A. Boltasseva, J. Guan, V. M. Shalaev, and A. V. Kildishev, "Refractory Plasmonics with Titanium Nitride: Broadband Metamaterial Absorber," Adv. Mater. **26**(47), 7959–7965 (2014).
25. Z.-Y. Yang, Y.-H. Chen, B.-H. Liao, and K.-P. Chen, "Room temperature fabrication of titanium nitride thin films as plasmonic materials by high-power impulse magnetron sputtering," Opt. Mater. Express **6**(2), 540 (2016).
26. C. M. Zgrabik and E. L. Hu, "Optimization of sputtered titanium nitride as a tunable metal for plasmonic applications,," Opt. Mater. Express **5**(12), 2786–2797 (2015).
27. B. W. Karr, I. Petrov, D. G. Cahill, J. E. Greene, B. W. Karr, I. Petrov, D. G. Cahill, and J. E. Greene, "Morphology of epitaxial TiN(001) grown by magnetron sputtering," Appl. Phys. Lett. **70**(13), 1703–1705 (1997).

Optical Materials EXPRESS

28. S. Logothetidis, I. Alexandrou, A. Papadopoulos, S. Logothetidis, and A. Papadopoulos, "In situ spectroscopic ellipsometry to monitor the process of TiNx thin films deposited by reactive sputtering," J. Appl. Phys. **77**(3), 1043–1047 (1995).
29. P. Patsalas, N. Kalfagiannis, and S. Kassavetis, "Optical Properties and Plasmonic Performance of Titanium Nitride," Materials **8**(6), 3128–3154 (2015).
30. P. Huber, D. Manova, S. Mandl, and B. Rauschenbach, "Optical characterization of TiN produced by metal-plasma immersion ion implantation,," Surf. Coat. Technol. **142-144**, 418–423 (2001).
31. C. Wiemera, F. Lévya, and F. Bussy, "Determination of chemical composition and its relationship with optical properties of Ti — N and Ti — V — N sputtered thin films," Surf. Coat. Technol. **68-69**, 181–187 (1994).
32. B. Karlsson, R. P. Shimshock, and B. O. Seraphin, "Optical properties of CVD-coated TiN, ZrN AND HfN," Sol. Energy Mater. **7**(4), 401–411 (1983).
33. G. V. Naik, J. Kim, and A. Boltasseva, "Oxides and nitrides as alternative plasmonic materials in the optical range [Invited]," Opt. Mater. Express **1**(6), 1090–1099 (2011).
34. I.-S. Yu, H.-E. Cheng, C.-C. Chang, Y.-W. Lin, H.-T. Chen, Y.-C. Wang, and Z.-P. Yang, "Substrate-insensitive atomic layer deposition of plasmonic titanium nitride films," Opt. Mater. Express **7**(3), 777 (2017).
35. S. Murai, K. Fujita, Y. Daido, R. Yasuhara, R. Kamakura, and K. Tanaka, "Plasmonic arrays of titanium nitride nanoparticles fabricated from epitaxial thin films," Opt. Express **24**(2), 1143 (2016).
36. 36. C. C. Chang, J. Nogan, Z. P. Yang, W. J. M. Kort-Kamp, W. Ross, T. S. Luk, D. A. R. Dalvit, A. K. Azad, and H. T. Chen, "Highly Plasmonic Titanium Nitride by Room-Temperature Sputtering," Sci. Rep. **9**(1), 1–9 (2019).
37. R. V. Babinova, V. V. Smirnov, A. S. Useenov, K. S. Kravchuk, E. V. Gladkikh, V. I. Shapovalov, and I. L. Mylnikov, "Mechanical properties of titanium nitride films obtained by reactively sputtering with hot target," J. Phys.: Conf. Ser. **872**, 012035 (2017).
38. S. Datta, M. Das, V. K. Balla, S. Bodhak, and V. K. Murugesan, "Mechanical, wear, corrosion and biological properties of arc deposited Titanium nitride coatings," Surf. Coat. Technol. **344**, 214–222 (2018).
39. X. Pang, L. Zhang, H. Yang, K. Gao, and A. A. Volinsky, "Residual Stress and Surface Energy of Sputtered TiN Films," J. Mater. Eng. Perform. **24**(3), 1185–1191 (2015).
40. W. R. Tyson, "Surface free energies of solid metals estimation from liquid surface tension measurements," Surf. Sci. **62**(1), 267–276 (1977).
41. J. A. Conway, S. Sahni, and T. Szkopek, "Plasmonic interconnects versus conventional interconnects: a comparison of latency, cross- talk and energy costs," Opt. Express **15**(8), 4474–4484 (2007).
42. A. Capretti, Y. Wang, N. Engheta, and L. D. Negro, "Comparative Study of Second-Harmonic Generation from Epsilon-Near-Zero Indium Tin Oxide and Titanium Nitride Nanolayers Excited in the Near-Infrared Spectral Range," ACS Photonics **2**(11), 1584–1591 (2015).
43. P. Berini, "Figures of merit for surface plasmon waveguides," Opt. Express **14**(26), 13030–13042 (2006).
44. R. Buckley and P. Berini, "Figures of merit for 2D surface plasmon waveguides and application to metal stripes," Opt. Express **15**(19), 12174–12182 (2007).
45. M. G. Blaber, M. D. Arnold, and M. J. Ford, "A review of the optical properties of alloys and intermetallics for plasmonics," J. Phys.: Condens. Matter **22**(14), 143201 (2010).
46. U. Guler, G. V. Naik, A. Boltasseva, V. M. Shalaev, and A. V. Kildishev, "Performance analysis of nitride alternative plasmonic materials for localized surface plasmon applications," Appl. Phys. B **107**(2), 285–291 (2012).
47. M. I. Stockman, "Nanoplasmonics: past, present, and glimpse into future," Opt. Express **19**(22), 22029–22106 (2011).
48. N. Kinsey, M. Ferrera, G. V Naik, V. E. Babicheva, and V. M. Shalaev, "Experimental demonstration of titanium nitride plasmonic interconnects," Opt. Express **22**(10), 12238–12247 (2014).
49. S. Ishii, S. L. Shinde, W. Jevasuwan, N. Fukata, and T. Nagao, "Hot Electron Excitation from Titanium Nitride Using Visible Light," ACS Photonics **3**(9), 1552–1557 (2016).
50. S. Podder and A. R. Pal, "Hot carrier devices using visible and NIR responsive titanium nitride nanostructures with stoichiometry variation," Opt. Mater. **97**, 109379 (2019).
51. L. Gui, S. Bagheri, N. Strohfeldt, M. Hentschel, C. M. Zgrabik, B. Metzger, H. Linnenbank, E. L. Hu, and H. Giessen, "Nonlinear Refractory Plasmonics with Titanium Nitride Nanoantennas," Nano Lett. **16**(9), 5708–5713 (2016).
52. S. Saha, A. Dutta, N. Kinsey, A. V Kildishev, V. M. Shalaev, and A. Boltasseva, "On-Chip Hybrid Photonic-Plasmonic Waveguides with Ultrathin Titanium Nitride Films,," ACS Photonics **5**(11), 4423–4431 (2018).
53. B. Saha, S. Saber, E. A. Stach, E. P. Kvam, and T. D. Sands, "Understanding the Rocksalt-to-Wurtzite phase transformation through microstructural analysis of (Al, Sc) N epitaxial thin films," Appl. Phys. Lett. **109**(17), 172102 (2016).
54. J. L. Schroeder, B. Saha, M. Garbrecht, N. Schell, T. D. Sands, and J. Birch, "Thermal stability of epitaxial cubic-TiN/(Al,Sc)N metal/ semiconductor superlattices," J. Mater. Sci. **50**(8), 3200–3206 (2015).
55. B. Saha, S. K. Lawrence, J. L. Schroeder, J. Birch, D. F. Bahr, and T. D. Sands, "Enhanced hardness in epitaxial TiAlScN alloy thin films and rocksalt TiN/(Al,Sc)N superlattices," Appl. Phys. Lett. **105**(15), 151904 (2014).
56. B. Saha, G. V. Naik, S. Saber, C. Akatay, E. A. Stach, V. M. Shalaev, A. Boltasseva, and T. D. Sands, "TiN/(Al,Sc)N metal/dielectric superlattices and multilayers as hyperbolic metamaterials in the visible spectral range," Phys. Rev. B **90**(12), 125420 (2014).

Optical Materials EXPRESS

57. Z. Jacob, I. I. Smolyaninov, and E. E. Narimanov, "Broadband Purcell effect: Radiative decay engineering with metamaterials," Appl. Phys. Lett. **100**(18), 181105 (2012).
58. M. N. Gadalla, K. Chaudhary, C. M. Zgrabik, F. Capasso, and E. L. Hu, "Imaging of surface plasmon polaritons in low-loss highly metallic titanium nitride thin films in visible and infrared regimes," Opt. Express **28**(10), 14536–14546 (2020).
59. W. A. Britton, Y. Chen, and L. D. Negro, "Double-plasmon broadband response of engineered titanium silicon oxynitride," Opt. Mater. Express **9**(2), 878–891 (2019).
60. Y. Krockenberger, S. Karimoto, H. Yamamoto, and K. Semba, "Coherent growth of superconducting TiN thin films by plasma enhanced molecular beam epitaxy," J. Appl. Phys. **112**(8), 083920 (2012).
61. W. Guo, R. Mishra, C. Cheng, B. Wu, L. Chen, M. Lin, and S. Gwo, "Titanium Nitride Epitaxial Films as a Plasmonic Material Platform: Alternative to Gold," ACS Photonics **6**(8), 1848–1854 (2019).
62. I. Krylov, X. Xu, Y. Qi, K. Weinfeld, V. Korchnoy, M. Eizenberg, and D. Ritter, "Effect of the substrate on structure and properties of titanium nitride films grown by plasma enhanced atomic layer deposition," J. Vac. Sci. Technol., A **37**(6), 060905 (2019).
63. P. V. Burmistrova, J. Maassen, T. Favaloro, B. Saha, S. Salamat, Y. R. Koh, S. Mark, A. Shakouri, and T. D. Sands, "Thermoelectric properties of epitaxial ScN films deposited by reactive magnetron sputtering onto MgO(001) substrates," J. Appl. Phys. **113**(15), 153704 (2013).
64. A. Achour, R. L. Porto, M. A. Soussou, M. Islam, M. Boujtita, K. A. Aissa, L. Le Brizoual, A. Djouadi, and T. Brousse, "Titanium nitride films for micro-supercapacitors: Effect of surface chemistry and film morphology on the capacitance," J. Power Sources (2015).
65. H. Fujiwara and R. W. Collins, *Spectroscopic Ellipsometry for Photovoltaics* (Springer, 2018), 1.
66. M. Silveirinha and N. Engheta, "Tunneling of electromagnetic energy through subwavelength channels and bends using ε-near-zero materials," Phys. Rev. Lett. **97**(15), 157403 (2006).
67. J. B. Khurgin, M. Clerici, V. Bruno, L. Caspani, C. DeVault, J. Kim, A. Shaltout, A. Boltasseva, V. M. Shalaev, M. Ferrera, D. Faccio, and N. Kinsey, "Adiabatic frequency shifting in epsilon-near-zero materials: the role of group velocity," Optica **7**(3), 226–2536 (2020).
68. S. Vezzoli, V. Bruno, C. Devault, T. Roger, V. M. Shalaev, A. Boltasseva, M. Ferrera, M. Clerici, A. Dubietis, and D. Faccio, "Optical Time Reversal from Time-Dependent Epsilon-Near-Zero Media," Phys. Rev. Lett. **120**(4), 043902 (2018).
69. V. Bruno, C. Devault, S. Vezzoli, Z. Kudyshev, T. Huq, S. Mignuzzi, A. Jacassi, S. Saha, Y. D. Shah, S. A. Maier, D. R. S. Cumming, A. Boltasseva, M. Ferrera, M. Clerici, D. Faccio, R. Sapienza, and V. M. Shalaev, "Negative Refraction in Time-Varying Strongly Coupled Plasmonic-Antenna – Epsilon-Near-Zero Systems," Phys. Rev. Lett. **124**(4), 043902 (2020).
70. Y. Zhou, M. Z. Alam, M. Karimi, J. Upham, O. Reshef, A. E. Willner, and R. W. Boyd, "Broadband frequency translation through time refraction in an epsilon-near-zero material," Nat. Commun. **11**(1), 2180 (2020).
71. N. Kinsey, C. DeVault, A. Boltasseva, and V. M. Shalaev, "Near-zero-index materials for photonics," Nat. Rev. Mater. **4**(12), 742–760 (2019).
72. M. Chirumamilla, A. Chirumamilla, Y. Yang, A. S. Roberts, P. K. Kristensen, K. Chaudhuri, A. Boltasseva, D. S. Sutherland, S. I. Bozhevolnyi, and K. Pedersen, "Large-Area Ultrabroadband Absorber for Solar Thermophotovoltaics Based on 3D Titanium Nitride Nanopillars," Adv. Opt. Mater. (2017).
73. C. Y. Young, "The frequency and temperature dependence of the optical effective mass of conduction electrons in simple metals," J. Phys. Chem. Solids **30**(12), 2765–2769 (1969).
74. R. N. Gurzhi, "On the Theory of the Infrared Absorptivity of Metals," J. Exptl. Theor. Phys. **33**, 660–668 6 (1958).
75. W. E. Lawrence and J. W. Wilkins, "Electron-Electron Scattering in the Transport Coefficients of Simple Metals," Phys. Rev. B **13**(6), 2717 (1976).
76. G. R. Parkins, W. E. Lawrence, and R. W. Christy, "Intraband optical conductivity σ(ω,T) of Cu, Ag, and Au: Contribution from electron-electron scattering," Phys. Rev. B **23**12), 6408–6416 (1981).
77. W. E. Lawrence, "Electron-electron scattering in the low-temperature resistivity of the noble metals," Phys. Rev. B **13**(12), 5316–5319 (1976).
78. R. T. Beach and R. W. Christy, "Electron-electron scattering in the intraband optical conductivity of Cu, Ag, and Au," Phys. Rev. B **16**(12), 5277–5284 (1977).
79. 12 H. Reddy, U. Guler, Z. Kudyshev, A. V. Kildishev, V. M. Shalaev, and A. Boltasseva, "Temperature-Dependent Optical Properties of Plasmonic Titanium Nitride Thin Films,," ACS Photonics **4**(6), 1413–1420 (2017).
80. J. A. Briggs, G. V. Naik, Y. Zhao, T. A. Petach, K. Sahasrabuddhe, D. Goldhaber-Gordon, N. A. Melosh, and J. A. Dionne, "Temperature-dependent optical properties of titanium nitride," Appl. Phys. Lett. **110**(10), 101901 (2017).
81. H. Reddy, U. Guler, A. V. Kildishev, A. Boltasseva, and V. M. Shalaev, "Temperature-dependent optical properties of gold thin films," Opt. Mater. Express **6**(9), 2776–2802 (2016).
82. S. T. Sundari, S. Chandra, and A. K. Tyagi, "Temperature dependent optical properties of silver from spectroscopic ellipsometry and density functional theory calculations," J. Appl. Phys. **114**(3), 033515 (2013).
83. S. A. Maier, *Plasmonics: Fundamentals and Applications* (Springer, 2007).
84. J. Homola, *Electromagnetic Theory of Surface Plasmons* (Springer, 2006).
85. A. Banerjee, R. M. Heath, D. Morozov, D. Hemakumara, U. Nasti, I. Thayne, and R. H. Hadfield, "Optical properties of refractory metal based thin films,," Opt. Mater. Express **8**(8), 2072 (2018).

Optical Materials EXPRESS

86. G. V Naik, J. L. Schroeder, X. Ni, V. Alexander, T. D. Sands, and A. Boltasseva, "Titanium nitride as a plasmonic material for visible and near-infrared wavelengths,," Opt. Mater. Express **2**(4), 478–489 (2012).
87. N. Fang, Z. Liu, T. Yen, and X. Zhang, "Regenerating evanescent waves from a silver superlens," Opt. Express **11**(7), 682–687 (2003).
88. P. B. Johnson and R. W. Christy, "Optical Constant of the Noble Metals," Phys. Rev. B **6**(12), 4370–4379 (1972).